Influence of Mg and Li content on the microstructure evolution of Al Cu Li alloys during long-term ageing

A. Deschamps, M. Garcia, J. Chevy, B. Davo, F. de Geuser

Influence of Mg and Li content on the microstructure evolution of Al-Cu-Li alloys during long-term ageing

A. Deschamps[1,2], M. Garcia[1,2,3], J. Chevy[3], B. Davo[3], F. De Geuser[1,2]

[1] Université Grenoble Alpes, SIMAP, F-38000 Grenoble, France
[2] CNRS, SIMAP, F-38000 Grenoble, France
[3] Constellium Technology Center, CS 10027, 38341 Voreppe Cedex, France

Abstract

The evolution of microstructure during long-term ageing (LTA) up to 3000h at 85°C following a T8 heat treatment has been characterised in three Al-Cu-Li-Mg alloys of variable Mg and Li content. A combination of transmission electron microscopy, differential scanning calorimetry and small-angle X-ray scattering has been used to evaluate the evolution of the different phases. In the T8 condition all three alloys contain a high density of T_1 precipitates together with S precipitates along the dislocations introduced by pre-stretching. In addition, the alloy with highest Li contains δ' precipitates. During LTA this last alloy experiences a significant complementary precipitation of δ'. The two other alloys experience a much more limited microstructure evolution, which appears to be linked to the formation and subsequent evolution of metastable phases (GP and GPB zones) in the regions between T_1 platelets. The evolution of the alloys' strength is shown to be well correlated to their microstructure.

1. Introduction

Al-Cu-Li alloys have experienced a strong development in the last 10 years for aerospace applications [1–4]. Following an initial development mostly restricted to spatial applications before 2000 [5], new chemical compositions, particularly reducing the Li level have emerged [6,7] and are now used in civil aircraft [8].

The range of alloy compositions currently of interest is still relatively large [9–19], with Cu generally around 3 wt%, Li contents ranging from 0.7 to 1.5 wt%, a wide range of Mg contents, and the addition of other species such as Ag or Zn. The precipitation sequence resulting from the chosen alloy composition can be complex, associating several paths of metastable and stable phases. A high level of Li favours the formation of the metastable δ' phase [6,20,21]. The association of Cu and Li favours the formation of the T_1 phase [22–24], which however relies on the presence of dislocations [25–30,19] and Mg [31–35], often complemented by Ag and/or Zn for an efficient nucleation. However, precipitates of the Al-Cu sequence (GP zones, θ'' and θ', usually) are frequently present as well [6,20,36,37]. In the presence of Mg, one can also find precipitates of the Al-Cu-Mg sequence (GPB zones, S'/S) [38–41]. Usually, it is considered that the best mechanical properties in these alloys are found when a majority of T_1 phase is formed [18,27,30]. Although increasing the Li content helps reaching even higher strength, the δ' phase is subject to shear localization due to its ordered, shearable nature, and therefore its presence is considered to be unfavourable to the alloy toughness and ductility [42].

One of the issues that limited the use of the Al-Cu-Li alloys of the first generation is that their microstructure was not stable during long term ageing (LTA) in service following a T8 ageing treatment. Particularly, high Li alloys were shown to be susceptible to microstructure evolution at temperatures below 100°C, due to the strong dependence of Li solubility as a function of temperature in this range, to the high mobility of Li and homogeneous nucleation of the δ' phase made possible by its coherent interface with the matrix. In the alloy C458, Ortiz and co-workers [43] showed a loss of fracture toughness of 40% after 955h at 135°C. Noble and Harris [44]

obtained similar results, namely a loss of toughness of 43% and an increase of yield strength of 10%, for ageing of 1000h at 100°C on a 2.5wt%Li containing Al-Cu alloy. Katsikis and co-workers [45] confirmed these results and showed that a 1000h ageing at 70°C resulted in a bi-modal distribution of δ' precipitates, the smaller ones being formed during low temperature ageing.

Until now, the study of the effect of long term ageing on microstructure and properties has been limited to alloys whose Li content was larger than 1.5 wt%. To our knowledge, there is no study in the literature of the alloy stability for lower Li content alloys, despite these alloys being the subject of the majority of the recent developments. Moreover, no study exists either on the effect of other solute elements, and in particular Mg, on the long-term ageing behaviour. Therefore, the aim of the present paper is to describe the response to long term ageing (subsequently named LTA, up to 3000h) at 85°C of three alloys, where the Li and Mg content are varied independently. The three triplets of (Cu,Li,Mg) contents (in wt%) investigated are (2.8,0.7,0.3) (that we will call base alloy), (2.3,1.4,0.3) (that we will call high Li alloy) and (2.7,0.8,0.6) (that we will call high Mg alloy). The microstructure of all alloys is first qualitatively described using Transmission Electron Microscopy (TEM). The quantification of microstructure evolutions is then achieved by combining Differential Scanning Calorimetry (DSC) and Small-Angle X-ray Scattering (SAXS). The resulting mechanical properties are evaluated by tensile tests.

2. Materials and experimental methods

The list of alloy compositions is presented in Table 1. In addition to the three main solute elements Cu, Li and Mg, all three alloys contain a comparable amount of Ag. They differ in terms of other solute elements (Fe, Si, Zr, Mn), however these elements, of very low diffusivity, control mainly the distribution of dispersoids and second phase particles, which are not expected to vary during long term ageing. However, the resulting grain structure of the three alloys is quite different, namely fully fibrous for the Base alloy, recrystallized for the High Li alloy and mixed for the High Mg alloy. This difference of grain structure will have some influence on the visualization of the precipitates in the SAXS images and on the mechanical properties.

Before long term ageing, the three alloys were subjected to a solution heat treatment adapted to each composition in order to dissolve undesired phases that could have precipitated during hot rolling and quenched into water at room temperature. A 2% to 3% deformation was then applied by stretching. Alloys were then aged to a T8 temper. Following this heat treatment, all long term ageing treatments were made in a single furnace at 85°C, in order to ensure the best reproducibility. Ageing times of 1000, 2000, and 3000h at 85°C have been investigated.

TEM samples were prepared by standard procedures of mechanical grinding followed by twin-jet electropolishing in a nitric acid-methanol solution. Different samples were prepared before and after long-term ageing, and observed using a FTEM Zeiss EM912 apparatus, which is equipped with an energy filter allowing for inelastically scattered electrons removal in electron diffraction patterns.

DSC samples were prepared after long term ageing experiments as 4mm diameter disks of typical weight 30-50 mg. Since only small variations in microstructure during long-term ageing are expected, a specific procedure for maximizing the data quality was adopted. First, the low temperature events (until 350°C) were evaluated with a TA200 apparatus, which presents a very stable baseline. Two successive scans were performed from -50°C to 350°C at 20°C/min, separated by cooling at 50°C/min. It is expected that after stabilisation of the microstructure at 350°C and cooling, no thermal events should occur during the second scan. This is valid until 250°C, where the signal deviates from the baseline, as shown in figure 1a. Thus, the baseline used for the first scan, was estimated by fitting the second scan until 250°C with a third order polynomial and extrapolating this polynomial to 350°C. This baseline includes both the instrumental baseline and the evolution of the sample heat capacity, so that the resulting signal originates from kinetics reactions only and should be close to zero when no reaction occurs. The resulting DSC thermograms will be shown in Figure 10 later in the paper.

In order to also access the higher temperature thermal events, a Perkin Elmer Pyris1 apparatus was used at the same heating rate, in the temperature range 40°C to 550°C. However, for this apparatus the baseline measurement using a reference sample is not reproducible enough to detect subtle differences arising during long-term ageing. Above roughly 480°C, the alloys are completely in solid solution, which provides a first estimate of the baseline. In the temperature range 40°C-250°C, the baseline was estimated by subtracting to the experimental data, the baseline-corrected data from the first set of experiments realized on the TA apparatus. The final baseline on the complete temperature range was then estimated by fitting a polynomial function on the two temperature ranges (40-250°C and 480-550°C), as shown in Figure 1b. The resulting thermograms will be shown in Figure 9 later in the paper. Using this procedure, the best baseline correction and highest data reproducibility was obtained, as will be shown in the results section.

SAXS experiments were performed with a rotating anode using a Cu Kα target. The beam size on the sample was approximately 1mm in diameter. The 2D SAXS patterns were collected at a distance of 574mm on a Dectris Pilatus 2 300k detector, giving access to scattering vectors ranging between 0.02 and 0.35 $Å^{-1}$.

Because precipitates in this system are usually non spherical (T_1, GP zones, θ' are platelets of high aspect ratio), the resulting SAXS patterns present characteristic streaks [46,47]. The distribution of these streaks and their intensity depends critically on the local distribution of grains probed by the X-ray beam, and of their texture. Therefore, measuring with a good precision the evolution of the precipitate microstructures during long-term ageing imposed to use a specific procedure to ensure that exactly the same sample volume would be probed before and after ageing in each sample. The samples were first prepared in the T8 state by mechanical polishing down to a thickness of approximately 80 µm. They were then placed in a sample holder and fixed mechanically. The sample holder was placed in the furnace at 85°C and removed for each set of measurements, before being placed in the furnace again for the next ageing sequence. The sample holder positioning with respect to the X-ray beam was estimated to be better than 100 µm. In order to ensure maximum data reproducibility, 900 measurements were made for each alloy and ageing condition, on a measurement grid with a step of 100 µm (thus totalling a measurement area of 3mm x 3mm). The 2D patterns that will be shown in the result section are selected individual images, and the integrated profiles are the sum of all collected data.

Mechanical tests were performed on samples following ASTM E8 standard. The sample thickness was 2.5 mm for the Base alloy and the high Mg alloy, and 5 mm for the high Li alloy. Tensile tests were both performed in the rolling direction (R) and in the transverse direction in the rolling plane (T). Three samples were tested for each condition, and the standard deviation of the measured yield strength was 2 MPa.

3. TEM analysis

3.1. Microstructure in T8 state

The identification of the hardening precipitation in the matrix was achieved with the help of the diffraction patterns according to three Al zone axes: [100], [110] and [112]. Figure 2 schematizes the expected diffraction patterns for the main phases that can be encountered during low-temperature ageing of these alloys (T_1 (Al_2CuLi), θ'(Al_2Cu)/GP zones, δ'(Al3Li) / β'(Al_3Zr), S/S'(Al_2CuMg)), whether as diffraction spots or as streaks when very thin and high aspect ratio precipitates are observed edge-on. Also, the placement of the apertures that will be used for the dark field micrographs is shown on these diagrams.

Figure 3, 4 and 5 shows the diffraction patterns in the three zone axes for respectively the base alloy, the high Mg alloy and the high Li alloy. In the T8 condition, all three alloys contain as the main precipitate the T_1 phase. Intense streaks are visible in the <110> and <112> axes, corresponding to edge-on T_1 particles. Other variants show strong diffraction spots in the three zone

axes. From the diffraction diagrams, it is also straightforward to identify the presence of the $L1_2$ phases, which could be a combination of β' and δ'. In the two low-Li alloys, these reflections have a relatively low intensity. Using electron dispersive X-ray spectroscopy (EDS) in the TEM revealed that the $L1_2$ precipitates in these two alloys were mostly β'. Back-scattered electrons imaging in a FEG-SEM confirmed that the spherical particles present in these two alloys have a larger average atomic weight than Al and therefore are β' precipitates. In the high Li alloy, however, these reflections are much more intense (typically more intense than that of the T_1 phase). Since this alloy contains a similar amount of Zr, thic increased intensity is related to the presence of a significant fraction of δ'.
The presence of precipitates of the Al-Cu family (GPI, GPII or θ') is best evaluated by the observation of the streaks along {002} reflections in the <100> or <110> zone axes. Such streaks are faintly observed in the base and high Mg alloys, but are difficult to detect in the high Li alloy.
Finally, the presence of the S'(S) phase can be detected both as a cross around the {011} forbidden reflections of the <100> zone axis, and as streaks along {221} reflections in the <112> zone axis. The diffraction patterns show that S'(S) phases are significantly present in the base and high Mg alloy, and to a lesser extent in the high Li alloy.

Figure 6, 7 and 8 show dark field images for the three alloys respectively taken in <110> zone axis with aperture DF1, in <110> zone axis with aperture DF2, and in <001> zone axis with aperture DF3 (see Figure 2 for placement of apertures). The dark field images made with aperture DF1 (Figure 6) show edge-on one out of the four variants of T_1. In all three alloys a dense distribution of such precipitates is found, with a projected diameter of 100 to 200 nm, showing that these particles are the main phase present in the T8 conditions in accordance with the diffraction patterns. Dark field images made with aperture DF2 (figure 7) show both the $L1_2$ precipitates and one out of 3 variants of the GP zones / θ' precipitates seen edge-on. Concerning the $L1_2$ precipitates in the base and high Mg alloy, it is difficult to conclude on the observed density. Zr being a slow-diffusing peritectic element in Al, its distribution is known to be very heterogeneous [48] so that some places may have a high density of β' and others almost none. However, the high Li alloy clearly shows a higher density of $L1_2$ precipitates, which can be attributed to the presence of δ' precipitates in the T8 condition, particularly as this alloy has a very low Zr content. In the three alloys in the T8 condition, very few GP zones / θ' precipitates are observed. However, in these alloys single layer GP zones can be stabilized in the T8 condition [6,42] and these may be invisible on conventional dark field micrographs. Finally, dark field micrographs made with aperture DF3 (Figure 8) enlighten both the $L1_2$ phases and the S'/S precipitates. For the latter, it appears to be present in all three alloys, particularly in the high Mg alloy, as expected for a Mg-containing phase. The S'/S precipitates delineate curved linear features that are clearly the dislocations introduced by pre-deformation prior to ageing.

3.2 Evolution during long-term ageing

Figures 3, 4, 5 and 6, 7, 8 show, along with the diffraction patterns / micrographs of the T8 condition, those after long-term ageing (LTA) of 2000h at 85°C.
Although the diffraction patterns cannot give quantitative information on the evolution of the different precipitate families, because the diffraction spots intensities depend on the local imaging conditions (sample thickness, tilt), they make it possible to delineate, if present, the significant changes that have happened due to the LTA.
For the base alloy, the diffraction patterns do not show any change in the phases present. All spots and streaks that were present in the T8 condition are still present after LTA, and no new reflections have appeared. The relative intensity of the reflections seems to be unchanged.
In the high Mg alloy, the same situation is observed. However, it seems from the <110> pattern that GP zones / θ' are more present after LTA as compared to the T8 condition.

For the high Li alloy, the evolution is more substantial. The major change is a strong increase of the $L1_2$ reflections, meaning that a complementary precipitation of δ' has happened. Besides, it seems that the intensity of the streaks corresponding to S'/S phase in the <112> zone axis has increased; however this is not accompanied by an increased in the S'/S reflections in the <001> zone axis so that it is difficult to conclude from diffraction patterns alone. The GP zones / θ' streaks are not observed in <110> zone axis, but are visible in the <001> zone axis both before and after ageing, so that again a more quantitative description of the microstructure is needed to determine finely the microstructure evolutions.

The observation of the dark field micrographs is consistent with the above-mentioned findings. Micrographs made with DF1 aperture show that no visible change of the T_1 precipitate distribution has occurred. Whether some subtle evolutions have occurred cannot be established by using the TEM results alone. Additional information requires complementary experimental techniques, which average on a larger amount of material, such as DSC or SAXS. These results are presented later in this paper.

Micrographs made with DF2 confirm, for the high Li alloy, that a new population of δ' precipitates has appeared during LTA. Along this new population, the micrograph suggests that the size of the pre-existing δ' has grown. A quantification by image analysis confirmed this impression: in the T8 condition the average radius of the δ' precipitates is equal to 10 nm, after LTA a clear bi-modal distribution was observed with respective average radii of 4 and 15 nm.

The dark field micrographs made with DF3 aperture do not show a drastic change in the morphology of the precipitates present at the dislocations. Although it seems that their presence has significantly progressed in the base alloy, it is not the case in the Li containing alloy, which is inconsistent with the reflections observed in the diffraction patterns. In fact, for this latter alloy, owing to the very high volume fraction of δ' precipitates present after LTA, the S'/S precipitates may be partly masked.

4. DSC analysis

4.1. T8 condition

Complementary to the TEM analysis, the initial microstructure has been characterised by DSC. The complete thermograms are shown in Figure 9 along with the thermograms after long-term ageing, which will be discussed in section 4.2.

The T8 state is a fully precipitated condition. Therefore, upon heating up to the solid solution temperature, one can expect mostly endothermic events, corresponding to the dissolution of the precipitates initially present. The magnitude of the dissolution peaks and their temperature of occurrence is representative of the thermal stability of the phases present in the T8 state [49,50]. Of course, some complementary precipitation can occur at higher temperature if some supersaturation is still present. Dorin et al. [51] studied by DSC and SAXS the evolution during continuous heating of an AA2198 Al-Cu-Li-Mg-Ag alloy in a condition similar to a T8 state (18h of ageing at 155°C), and found a secondary precipitation peak between 300 and 350°C corresponding to an increase of the T_1 precipitate volume fraction due to the activation of platelet thickening. They also found another secondary precipitation peak between 350 and 400°C corresponding to the precipitation of the θ' phase. Of course, these two secondary precipitation peaks were superimposed with a broad dissolution peak corresponding to the dissolution of the precipitate microstructure (mainly T_1 phase in this case).

Such behaviour is very similar to that observed in our Base alloy, as shown in Figure 9. A broad dissolution peak is present, starting around 160°C and ending around 470°C. On top of this dissolution one finds two secondary exothermic peaks, whose temperatures correspond to the two events cited above. It is visible that the broad dissolution peak contains significant events at relatively low temperatures (160-300°C) and a second, more clearly defined peak between 360 and

470°C. Based on the literature, the latter can be identified as the main dissolution peak for the T_1 phase. The broad low temperature peak is related to less stable phases, thus probably metastable ones. These may be Cu-containing GP zones, which are known to be present in this ageing state, and Mg-containing phases such as remaining Cu-Mg clusters [52].
Concerning now the Mg-rich alloy, we can see a first sequence of endothermic events in the temperature range 150-320°C, and then a two-stage dissolution peak until full dissolution. The first two peaks can be more clearly observed on the low temperature data shown in Figure 10. From the comparison with the extensive literature on Al-Cu-Mg alloy, it is likely that one of the two dissolution peaks (probably the second one) corresponds to the reversion of GPB zones still present after the T8 treatment [53,54]. Around 310°C, a small exothermic peak is observed which is very similar to that observed in the Base alloy, which corresponds most likely to the thickening of the T_1 precipitates. As for the main dissolution peak (Figure 9), it is striking that it presents a very different shape as compared to the Base alloy. In the higher temperature region of this peak (above 400°C) where the solute mobility is very high (after the maximum heat flow recorded), the alloy is expected to be close to equilibrium and therefore the shape of the peak is representative of the shape of the solvus boundary. Thus, the relatively modest change in Mg concentration results in a large change of the solvus boundary and therefore in the fraction of equilibrium phases in the alloy.

The Li-rich alloy presents a series of endothermal peaks. A first endothermal peak is observed at very low temperature (about 100°C), followed by a second peak between 180 and 250°C, and last the main dissolution peak with the usual complex sub-structure similarly to that found in the base alloy. The low-temperature endothermic peak has been observed before in Al-Li binary alloys [55–57]. In-situ X-ray diffraction experiments on {100} forbidden reflections has shown that this peak is related to a disordering process of the partially ordered Al-Li solid solution. Actually, this disordering peak can be also observed faintly in the Base and high Mg alloys on the low temperature data (Figure 10). The second dissolution peak centred on 230°C, clearly represents the dissolution of the δ’ precipitates present in the initial microstructure. Then, the main dissolution peak at high temperature corresponds to the dissolution of all other phases, mainly T_1.

4.2. Evolution during long-term ageing

As shown in figure 9, the DSC thermogram of the base alloy is barely modified by long-term ageing. The main high temperature dissolution peak is unchanged, so that it can be concluded that the equilibrium phases present in the T8 state (particularly T_1 precipitates) are unaffected by long-term ageing. However, this is not the case for the lower temperature thermal events. Their behaviour can be better observed in figure 10, which shows the thermograms obtained with a more precise baseline correction. The broad dissolution peak that we have attributed to the presence of Cu GP zones and Mg containing phases, shows a non-monotonous evolution with ageing time. It evolves in a self-similar manner, with a magnitude increase from 0 to 2000h, followed by a decrease at 3000h. Together with this behaviour, a similar modification is observed in the secondary exothermic peak at 350°C, which has been attributed to the formation of θ’. Dorin et al. [51] have shown in a similar alloy that in an ageing condition similar to a T8 state, a significant supersaturation in Cu was still present in between the main T_1 precipitating phase, which could be precipitated during heating of the alloy at higher temperature by the activation of the thickening of T_1 platelets. Therefore, they concluded that this Cu supersaturation was due to the specific nature of the growth of the T_1 platelets during initial T8 ageing, namely planar growth as single unit cell precipitates, which cannot give access to the whole solute field present in the microstructure. This planar growth stops by hard or soft impingement of the T_1 precipitates, and the remaining Cu in between the platelets is trapped until it precipitates as other phases or until thickening of the T_1 platelets is activated. It has actually been observed that Cu GP zones are present in between T_1 precipitates already in the T8 condition [6,42], and the low temperature dissolution peak of the T8 base alloy can be, at least partially, attributed to their presence.

Lowering the ageing temperature from the T8 ageing temperature (155°C) to the long term ageing temperature (85°C) actually increases further this Cu supersaturation, which can activate the further formation of these GP zones. It might then seem surprising that the magnitude of the DSC dissolution peak decreases at 3000h of ageing. Actually, this can be simply understood if one hypothesizes that the GP zones progressively transform into more stable phases (mainly θ') when given sufficient ageing time at 85°C. Then we can state that the sequence of events during long-term ageing is likely to be a complementary precipitation of GP zones, followed in a second stage by their transformation to θ'. Finally, one can notice on figure 10 that the faint disordering peak at 110°C disappears during long-term ageing in the Base alloy. Although it is difficult to draw firm conclusions from this fact, this may be the sign of a decrease of the Li content in solid solution. This Li could go to δ' precipitates or be associated with Cu-rich precipitates forming during ageing, particularly with θ', which is well known to become wetted by δ' in these alloys [6,20,40].
Considering now the high Mg alloy, we can see that the evolution during long-term ageing is very similar to that of the Base alloy. Similarly, the high temperature peaks are not significantly affected by the ageing time. As for the low temperature peaks, one can observe a strong increase of the first and second dissolution peaks. However, this increase is non monotonous, similarly to the situation in the base alloy, indicating that some of the objects formed during 85°C ageing are transformed into more stable phases for long ageing times. In this alloy too, the disordering peak at 110°C almost completely disappears (monotonically) during ageing. This behaviour, much more pronounced than in the Base alloy, is probably the sign of a decrease of the amount of Li in solid solution.

Finally, the behaviour of the Li-rich alloy presents by far the most spectacular evolution during ageing. Again, in this alloy the high temperature behaviour is unchanged by ageing (except for the 3000h case, where the baseline correction seems to be imperfect as shown by the thermogram above the solvus temperature), consistently with the expected fact that the equilibrium phases are unchanged by low-temperature ageing. At temperatures below 320°C, however, the evolution of the signal is dramatic, with a strong evolution of the endothermic peaks, which can be better visualized on the low-temperature data in Figure 10. The endothermic peak corresponding to the dissolution of δ' precipitates becomes a double peak, with the apparition of a second peak at lower temperature, together with an increase of the magnitude of the initial peak. The TEM observations have shown that during ageing this alloy developed a bi-modal δ' distribution, with large ones corresponding to that formed during T8 ageing and small ones nucleated during 85°C ageing. Since the small precipitates are thermodynamically less stable than the large ones, their dissolution peak must be at lower temperature. Therefore, the observed behaviour is good agreement with the formation of a bi-modal δ' distribution. From our data it is apparent that the initially present δ' precipitates do change also during ageing, since the endothermal events between 250 and 320°C strongly evolve also during 85°C ageing. Finally, the data in Figure 10 also shows a strong decrease of the low temperature dissolution peak at 110°C, which comes along with the increased fraction of δ'. This is again consistent with the attribution of this peak to the disordering of the Al-Li solid solution.

5. SAXS analysis

Figure 11 shows representative SAXS images of the three alloys, for the initial states until the 3000h of ageing at 85°C. The initial images are typical of the scattering induced by a majority of thin platelets, whose scattering appears as streaks in the reciprocal space. The distribution of these streaks is very different from one alloy to the other. Actually, it depends on the orientation of the grains probed by the X-ray beam with respect to the beam direction [47,58]. The base alloy has a fully fibrous structure, due to the presence of Zr and to the specific rolling schedule. Such a fibrous structure results in a texture presenting some well defined streaks, similar to those that have been observed in AA2198 alloy of similar grain structure before [6,29,30,46,51]. In contrast, the Li rich alloy shows a higher number of streaks oriented in seemingly random directions, representative of a

more random texture. This alloy, due to the Mn content in particular, has a recrystallized grain structure. The high Mg alloy, with its mixed structure, shows images that are intermediate between the two others.

In addition to the streaks, it is possible to distinguish in the high Li alloy an isotropic halo, which is absent from the two other alloys, and which seems to evolve with ageing time. This halo is characteristic of the δ' precipitates. However it is difficult to deconvolute this isotropic scattering from the streaks.

Scattering curves were obtained for each of these conditions by radial averaging of each image and then averaging 900 images per alloy and ageing state. Such averaged curves, representing precisely the same volume of the sample thanks to the procedure followed for the measurement, are shown in figure 12.

For the base alloy in the T8 condition, the scattering curve is typical of a microstructure dominated by platelet precipitates, with a low-q (where q is the scattering vector) behaviour as q^{-2}, and a large-q behaviour tending towards q^{-4}. The transition between the two regimes happens at a scattering vector of about 1/t where t is the platelet thickness [47], which is consistent with the known thickness of T_1 precipitates in the T8 condition of approximately 1 nm. Long-term ageing does not change much these scattering curves. A small but consistent increase is observed with progressing ageing time up to 3000h. This increase is well distributed across all the scattering angles, slightly more at small scattering vectors.

For the high Mg alloy in the T8 condition, the scattering behaviour is close to that of the base alloy, however with a less pronounced transition between the low- and high-q regimes. This suggests that the precipitates are still mostly elongated particles, but that the average thickness has values that are more distributed and not centred on a precise value as it is the case in the base alloy. This is consistent with the fact that the high Mg alloy has a larger fraction of S'/S precipitates, whose thickness may be larger than the 1 nm of the T_1 precipitates. During LTA, the scattering behaviour evolves almost in a self-consistent manner, suggesting that the phases that form have a similar shape as the phases initially present.

The Li-rich alloy presents the strongest evolution. The addition of the signal originating from the spherical δ' and the platelet-like T_1 precipitates gives a signal more difficult to interpret in the T8 condition. However, LTA results in a clear increase of the scattering curve, consistently with the evidence of the formation of new precipitates. We present in Figure 13 a Kratky plot ($I.q^2$ *vs.* q where I is the scattered intensity) of the difference between the SAXS signal after and before ageing. Implicitly, this representation is meaningful only if the precipitates initially present do not evolve during ageing, so that the difference in scattering can be related to the new precipitates formed. We know that this is not strictly true, due to the coarsening of the pre-existing δ' precipitates. However, as a first approximation, this representation should still provide a good estimate of the nature and fraction of δ' formed. This data shows that a well-defined signal develops during ageing with a clear peak in $I.q^2$, consistently with the formation of spherical precipitates. The average size of the precipitates calculated from this signal [59] is shown in Table 2. It increases gradually with ageing time, and the radius measured after 2000h (4.5 nm) corresponds particularly well with that of the small precipitates measured by TEM (mean radius of 4 nm). The integrated intensity calculated from the Kratky curves of Figure 15 is also given in Table 2. To convert this intensity in volume fraction, it is necessary to estimate the composition of the δ' precipitates. We will use the same assumption as in [57], namely a composition of Li of 23.5%. Then the same equations as in [57] can be used to calculate the precipitate volume fraction formed from the integrated intensity which provides a volume fraction of secondary δ' which increases with ageing time to reach 10% after 3000h of ageing (Table 2).

6. Evolution of yield strength during long-term ageing

Since the three alloys have a different grain structure (linked to the different Zr and Mn contents), it is desirable to average the texture effects on the evolution of yield strength. Therefore, mechanical

testing was realised both in the long (L) and long transverse (LT) directions and we will show an average of the two results.

Figure 14 shows the evolution of this average yield stress with ageing time. In the T8 condition, the base alloy is the strongest, and the high Li alloy shows the lowest yield strength. After 3000h of ageing, the base alloy's yield strength has varied very little, by less than 20 MPa. The high Mg alloy shows a somewhat larger variation, around 30 MPa. The high Li alloy shows the largest variation of the order of 60 MPa. In the end condition of 3000h at 85°C, the three alloys have almost the same yield strength.

7. Discussion

From the combination of transmission electron microscopy, differential scanning calorimetry and small-angle X-ray scattering, we have at our disposal a thorough characterization of the microstructure of the three alloys and their variation during the long term ageing heat treatment at 85°C. Before discussing the effect of LTA on microstructure it is worth summarizing the similarities and differences between the initial T8 microstructures.

Transmission electron microscopy shows that the three alloys present qualitatively the same main phases, except for the high Li alloy, which includes already δ' precipitates in the T8 condition. In the three alloys T_1 platelets are present with a high density, along with a comparatively lower fraction of S'/S precipitates along the dislocations introduced in the material during pre-deformation, and a low number density of θ'. Due to the higher Mg content in the high Mg alloy, it can be expected that this alloy presents a higher fraction of S precipitates. Actually, the high temperature behaviour in differential scanning calorimetry (above roughly 400°C) shows that the distribution of equilibrium phases is significantly different in the high Mg and in the base alloys, confirming that the proportion of S phase is higher.

The yield stresses from the different alloys are related to the strengthening role of the different phases. In the T8 condition, the base alloy has the highest yield stress. The high Mg alloy has a lower yield stress despite a similar Cu content, a similar Li content and a higher Mg content (and thus a higher total solute content). Since the S phase composition is Al_2CuMg, the additional Mg content in this alloy traps some Cu which is not available for the formation of T_1 (Al_2CuLi). From this it can be inferred that the strengthening capacity of the S phase is much lower than that of the T_1 phase. Actually, the S-containing alloys such as AA2024 present a comparatively lower strength in the artificially aged condition as compared to the Al-Cu-Li alloys [60] and are usually used in a naturally aged temper. The high Li alloy shows the lowest yield strength out of the three. Compared to the base alloy, it has a lower Cu content and a higher Li content. We have seen that it contained in the T8 condition δ' precipitates, but due to the lower Cu content the T_1 precipitate volume fraction will be smaller than that of the base alloy. Therefore, the lower yield strength of this alloy confirms that δ' precipitates are much less effective strengtheners as compared to T_1 precipitates.

The DSC analysis of the T8 condition shows that there is more in these alloys than only the main phases identified by electron microscopy. A series of low-temperature (i.e. 100-300°C) endothermal events shows that other metastable phases exist in this condition, some of which are not visible in the conventional dark field micrographs or in the energy-filtered electron diffraction patterns. First, the three alloys present a small endothermal peak around 100°C, which is most pronounced in the high Li alloy, smaller in the high Mg alloy and very faint in the base alloy. Based on former work in Al-Li binary alloys [55,56], this peak can be related to the loss of a partial Li ordering in solid solution. It can be inferred from its relatively high value in the high Li alloy that a large fraction of the Li is still available in solid solution after T8 ageing, reflecting the high Li solubility at the ageing temperature of 155°C [61,62].

More importantly, all three alloys show large endothermic peaks below 300°C. As shown in [51], T_1 precipitates are not expected to dissolve until larger temperatures. The small exothermic peak superimposed on the global endothermic behaviour at 320°C is related to the thickening of T_1 phase, and dissolution of this phase occurs yet at higher temperature. Similarly, the dissolution of

the S phase does not occur before 350°C. In the high Li alloy, this endothermal peak can be safely ascribed to the dissolution of δ' precipitates, because of the large solubility variation with temperature of Li in Al. In the two other alloys, however, these dissolution events must correspond to other metastable objects. Cu-rich GPI zones are actually expected in the T8 condition of such alloys. Besides, Cu-Mg clusters are known to form very rapidly in these alloys [63], and may evolve to GPB zones. Upon heating, these clusters or GPB zones partially revert around 250°C[64], which corresponds quite well to the temperature range identified in the present DSC scans. The reason for which low-temperature metastable precipitates may be present in the T8 condition along with more stable phases has to do with the particular geometry and nucleation mode of the main precipitates in these alloys. Both S phase and T_1 phase nucleate on the dislocations. The S phase does not grow to large sizes, as observed in detail by [65], presumably due to a shortage of Mg atoms, and therefore remains in the regions immediately around the dislocations (see Figure 8). The T_1 phase rapidly grows, but only a platelets of a thickness of a single unit cell at the temperature of 155°C. Therefore, at the end of the T8 artificial ageing treatment, a large proportion of the material remains out of range for the diffusion field of the limiting species, namely Cu. When the alloy is cooled down to ambient temperature, these regions supersaturated in Cu can evolve, forming clusters or GP / GPB zones, together when available with the remaining Mg.

Now we can discuss the evolution of these initial microstructures with ageing at the intermediate temperature of 85°C.

A global view of the microstructural evolutions can be obtained from the DSC data. This data shows that the equilibrium phase distribution, represented by the high temperature dissolution peak before full solutionizing, are very little modified during long term ageing. Since the equilibrium volume fraction is dominated by the dense distribution of T_1 precipitates, as shown by the TEM images, this stability is not surprising. Actually, it is now well established that at moderate temperatures in pre-deformed Al-Cu-Li alloys forming T_1 precipitates, these particles form quickly at constant thickness [6,30] until their growth is limited by soft and hard impingement, reaching a stable microstructure state. The remaining supersaturation in between the grown T_1 platelets can serve to form other metastable clusters or phases (see previous paragraph), but becomes accessible to T_1 precipitates only is temperature is above a critical value necessary for nucleating the extra ledge necessary for T_1 thickening. This T_1 thickness increase is extremely slow at 155°C (several hundred hours) [30], so that it is expected to be negligible during long term ageing at 85°C.

The less stable phases present in the microstructure, are represented by the low-temperature dissolution events in the DSC data. These phases evolve significantly with long-term ageing, to a limited extent for the base alloy, moderately for the high Mg alloy and strongly for the high Li alloy. In addition, the low-temperature dissolution evolution of the DSC scans is non-monotonous with ageing time for the two first alloys, whereas it increases monotonically for the high Li alloy. The effect of LTA on this last alloy is quite simple to understand as it is very clear from the TEM images, namely it is dominated by the formation of additional δ' precipitates on top of the ones pre-existing in the T8 condition. The remaining supersaturation left in Li after the T8 treatment can be simply understood from the evolution of Li solubility between 155°C and 85°C. According to Garland and Sanchez [61] and Noble and Bray [62] the solubility difference between these two temperatures in a binary Al-Li alloy is of the order of 2 at%, corresponding to a possibility to form an extra volume fraction of 8.5% if we consider a constant Li concentration of 23.5% in the precipitates. Although the situation will certainly be somewhat different in a complex Al-Cu-Li alloy, this is close from the 10% extra precipitates measured in the present work by SAXS. Interestingly, the supersaturation appears to be sufficient to nucleate new δ' precipitates in between the pre-existing ones, while these coarsen at the same time. The resulting strengthening increment is significant, of the order of 50 MPa. In parallel to this formation of δ' during LTA, other precipitate evolutions may happen, however they could not be resolved by TEM and appear to be hidden by the aforementioned precipitation reaction.

The effect of LTA on the two other alloys is very different, both quantitatively and qualitatively. First it is much smaller in magnitude: the microstructure evolution can only be detected by very sensitive measurements. In the TEM no evolution is observed, either by imaging or by diffraction. Only with the specific baseline correction of the DSC was it possible to observe a consistent evolution of the signal, and the SAXS data evolution required very careful measurements, ensuring that exactly the same sample area was measured for each ageing condition, and making the average between 900 images for each condition. In parallel, only 10 MPa (base alloy) and 20 MPa (high Mg alloy) strength evolution are observed, confirming the good stability of these alloys when subjected to LTA at 85°C. However, small changes occur in the low-temperature regions of the DSC scan, consistently with the evolution of the SAXS signal, which is distributed widely in terms of scattering vectors. This last feature corresponds well to additional features of high aspect ratio such as rods or platelets. Knowing that some degree of supersaturation of the species limiting T_1 precipitation, namely Cu, remains in between the platelets, it can be expected to precipitate as metastable phases during LTA. Depending on the level of Mg in the alloy, a significant level of this species may also be present in the microstructure, since it precipitates along with Cu in T_1. Therefore, a combination of Cu (GPI, GPII zones) and Cu-Mg (clusters, GPB zones) can be expected to form during LTA in the two alloys, with a higher proportion of the latter in the high Mg alloy. The fact that the low-temperature dissolution effect in DSC is non-monotonous, whereas the increase of SAXS intensity or strength is monotonous suggests that during the course of LTA, metastable phases form first and then start to transform to more stable phases (like θ' or S).

8. Conclusion

Using a combination of systematic transmission electron microscopy along with more global techniques (SAXS, DSC and yield strength measurements), the microstructural evolution and related strength evolution has been characterised during long-term ageing (LTA) up to 3000h at 85°C in three alloys of the Al-Cu-Li-Mg family with different combinations of Cu, Li and Mg.

In the T8 condition, the microstructure of the three alloys is dominated by the presence of the T_1 phase. Along with these platelets, the S phase is present along the dislocations introduced by pre-deformation. In addition, the high Li alloy contains an initial distribution of δ' precipitates.

Depending on the alloy composition, the microstructure shows a very different level of stability during LTA. The high Li alloy precipitates an additional fraction of δ' precipitates of the order of 10%, whereas the two other alloy only form a limited amount of metastable phases in the volumes in between the T_1 precipitates. This reflects in the strength evolution, which is largest in the high Li alloy. However, the base alloy has in the T8 condition the highest strength due to the high strengthening capacity of the T_1 phase, so that after 3000h at 85°C the three alloys show a comparable level of strength.

References

[1] J.C. Williams, E.A. Starke, Progress in structural materials for aerospace systems, Acta Mater. 51 (2003) 5775–5799. doi:10.1016/j.actamat.2003.08.023.

[2] T. Warner, Recently-developed aluminium solutions for areospace applications, Mater. Sci. Forum. 519-521 (2006) 1271–1278.

[3] R.J. Rioja, J. Liu, The Evolution of Al-Li Base Products for Aerospace and Space Applications, Metall. Mater. Trans. -Phys. Metall. Mater. Sci. 43A (2012) 3325–3337. doi:10.1007/s11661-012-1155-z.

[4] T. Dursun, C. Soutis, Recent developments in advanced aircraft aluminium alloys, Mater. Des. 56 (2014) 862–871. doi:10.1016/j.matdes.2013.12.002.

[5] E.. Starke Jr., J.T. Staley, Application of modern aluminium alloys to aircraft, Prog. Aerosp. Sci. 32 (1996) 131–172.

[6] B. Decreus, A. Deschamps, F. De Geuser, P. Donnadieu, C. Sigli, M. Weyland, The influence of Cu/Li ratio on precipitation in Al-Cu-Li-x alloys, Acta Mater. 61 (2013) 2207–2218.

[7] B. Malard, F. De Geuser, A. Deschamps, Microstructure distribution in an AA2050 T34 friction stir weld and its evolution during post-welding heat treatment, Acta Mater. 101 (2015) 90–100. doi:10.1016/j.actamat.2015.08.068.
[8] P. Lequeu, K.P. Smith, A. Danielou, Aluminum-Copper-Lithium Alloy 2050 Developed for Medium to Thick Plate, J. Mater. Eng. Perform. 19 (2010) 841–847. doi:10.1007/s11665-009-9554-z.
[9] M. Starink, N. Gao, N. Kamp, S. Wang, P. Pitcher, I. Sinclair, Relations between microstructure, precipitation, age-formability and damage tolerance of Al-Cu-Mg-Li (Mn, Zr, Sc) alloys for age forming, Mater. Sci. Eng. -Struct. Mater. Prop. 418 (2006) 241–249. doi:10.1016/j.msea.2005.11.023.
[10] H. Li, Y. Tang, Z. Zeng, Z. Zheng, F. Zheng, Effect of ageing time on strength and microstructures of an Al-Cu-Li-Zn-Mg-Mn-Zr alloy, Mater. Sci. Eng. -Struct. Mater. Prop. Microstruct. Process. 498 (2008) 314–320. doi:10.1016/j.msea.2008.08.001.
[11] Y. Lin, Z. Zheng, S. Li, X. Kong, Y. Han, Microstructures and properties of 2099 Al-Li alloy, Mater. Charact. 84 (2013) 88–99. doi:10.1016/j.matchar.2013.07.015.
[12] M.J.-F. Guinel, N. Brodusch, G. Sha, M.A. Shandiz, H. Demers, M. Trudeau, S.P. Ringer, R. Gauvin, Microscopy and microanalysis of complex nanosized strengthening precipitates in new generation commercial Al-Cu-Li alloys, J. Microsc. 255 (2014) 128–137. doi:10.1111/jmi.12143.
[13] S. Zhang, W. Zeng, W. Yang, C. Shi, H. Wang, Ageing response of a Al-Cu-Li 2198 alloy, Mater. Des. 63 (2014) 368–374. doi:10.1016/j.matdes.2014.04.063.
[14] Z. Gao, J.Z. Liu, J.H. Chen, S.Y. Duan, Z.R. Liu, W.Q. Ming, C.L. Wu, Formation mechanism of precipitate T-1 in AlCuLi alloys, J. Alloys Compd. 624 (2015) 22–26. doi:10.1016/j.jallcom.2014.10.208.
[15] S.J. Kang, T.-H. Kim, C.-W. Yang, J.I. Lee, E.S. Park, T.W. Noh, M. Kim, Atomic structure and growth mechanism of T-1 precipitate in Al-Cu-Li-Mg-Ag alloy, Scr. Mater. 109 (2015) 68–71. doi:10.1016/j.scriptamat.2015.07.020.
[16] H.Y. Li, W. Kang, X.C. Lu, Effect of age-forming on microstructure, mechanical and corrosion properties of a novel Al-Li alloy, J. Alloys Compd. 640 (2015) 210–218. doi:10.1016/j.jallcom.2015.03.212.
[17] J. Li, P. Liu, Y. Chen, X. Zhang, Z. Zheng, Microstructure and mechanical properties of Mg, Ag and Zn multi-microalloyed Al-(3.2-3.8)Cu-(1.0-1.4)Li alloys, Trans. Nonferrous Met. Soc. China. 25 (2015) 2103–2112. doi:10.1016/S1003-6326(15)63821-3.
[18] X. Fan, Z. He, P. Lin, S. Yuan, Microstructure, texture and hardness of Al-Cu-Li alloy sheet during hot gas forming with integrated heat treatment, Mater. Des. 94 (2016) 449–456. doi:10.1016/j.matdes.2016.01.001.
[19] B.I. Rodgers, P.B. Prangnell, Quantification of the influence of increased pre-stretching on microstructure-strength relationships in the Al-Cu-Li alloy AA2195, Acta Mater. 108 (2016) 55–67. doi:10.1016/j.actamat.2016.02.017.
[20] R. Yoshimura, T.J. Konno, E. Abe, K. Hiraga, Transmission electron microscopy in the early stages of precipitates in aged Al-Li-Cu alloys, Acta Mater. 51 (2003) 2891–2903.
[21] A.K. Khan, J.S. Robinson, Effect of silver on precipitation response of Al-Li-Cu-Mg alloys RID D-1730-2009, Mater. Sci. Technol. 24 (2008) 1369–1377. doi:10.1179/174328408X262391.
[22] S. Van Smaalen, A. Meetsma, J.L.D. Boer, P.M. Bronsveld, Refinement of the crystal structure of hexagonal Al2CuLi, J. Solid State Chem. 85 (1990) 293–298.
[23] P. Donnadieu, Y. Shao, F. De Geuser, G.A. Botton, S. Lazar, M. Cheynet, M. de Boissieu, A. Deschamps, Atomic structure of T-1 precipitates in Al-Li-Cu alloys revisited with HAADF-STEM imaging and small-angle X-ray scattering, ACTA Mater. 59 (2011) 462–472. doi:10.1016/j.actamat.2010.09.044.
[24] C. Dwyer, M. Weyland, L.Y. Chang, B.C. Muddle, Combined electron beam imaging and ab initio modeling of T(1) precipitates in Al-Li-Cu alloys, Appl. Phys. Lett. 98 (2011) 201909. doi:10.1063/1.3590171.
[25] W.A. Cassada, G.J. Shiflet, E.A.J. Starke, The effect of plastic deformation on Al2CuLi

(T1) precipitation, Metall. Trans. A. 22A (1991) 299–306.
[26] K.S. Kumar, S.A. Brown, J.R. Pickens, Microstructural evolution during aging of an Al_Cu_Li_Ag_Mg_Zr alloy, Acta Mater. 44 (1996) 1899–1915.
[27] B.M. Gable, A.W. Zhu, A.A. Csontos, E.A.J. Starke, The role of plastic deformation on the competitive microstructural evolution and mechanical properties of a novel Al-Cu-Li-X alloy, J. Light Met. 1 (2001) 1–14.
[28] A.K. Khan, J.S. Robinson, Effect of cold compression on precipitation and conductivity of an Al-Li-Cu alloy, J. Microsc. 232 (2008) 534–538. doi:10.1111/j.1365-2818.2008.02116.x.
[29] B. Decreus, A. Deschamps, F. de Geuser, C. Sigli, Influence of Natural Ageing and Deformation on Precipitation in an Al–Cu–Li Alloy, Adv. Eng. Mater. 15 (2013) 1082–1085. doi:10.1002/adem.201300098.
[30] T. Dorin, A. Deschamps, F. De Geuser, C. Sigli, Quantification and modelling of the microstructure/strength relationship by tailoring the morphological parameters of the T1 phase in an Al–Cu–Li alloy, Acta Mater. 75 (2014) 134–146. doi:10.1016/j.actamat.2014.04.046.
[31] S.P. Ringer, B.C. Muddle, I.J. Polmear, Effects of cold work on precipitation in Al-Cu-Mg-(Ag) and Al-Cu-Li-(Mg-Ag) alloys, Metall. Mater. Transcations A. 26A (1995) 1659–1671.
[32] G. Itoh, Q. Cui, M. Kanno, Effects of a small addition of magnesium and silver on the precipitation of T1 phase in an Al—4%Cu—1.1%Li—0.2%Zr alloy, Mater. Sci. Eng. A. 211 (1996) 128–137.
[33] D.L. Gilmore, E.A.J. Starke, Trace elements effects on precipitation processes and mechanical properties in an Al-Cu-Li alloy, Metall. Mater. Transcations A. 28A (1997) 1399–1415.
[34] B.P. Huang, Z.Q. Zheng, Independent and combined roles of trace Mg and Ag additions in properties precipitation process and precipitation kinetics of Al–Cu–Li–(Mg)–(Ag)–Zr–Ti alloys, Acta Mater. 46 (1998) 4381–4393.
[35] M. Murayama, K. Hono, Role of Ag and Mg on precipitation of T1 phase in an Al-Cu-Li-Mg-Ag alloy, Scr. Mater. 44 (2001) 701–706.
[36] B.M. Gable, M.A. Pana, G.J. Shiflet, E.A. Starke, The role of trace additions on the T1 coarsening behaviour in Al-Li-Cu-X alloys, Mater. Sci. Forum. 396-402 (2002) 699–704.
[37] R. Yoshimura, T.J. Konno, E. Abe, K. Hiraga, Transmission electron microscopy study of the evolution of precipitates in aged Al–Li–Cu alloys: the θ′ and T1 phases, Acta Mater. 51 (2003) 4251–4266.
[38] S.C. Wang, M.J. Starink, Precipitates and intermetallics phases in precipitation hardening Al-Cu-Mg-(Li) based alloys, Int. Mater. Rev. 50 (2005) 193–215.
[39] H. Djaaboube, D. Thabet-Khireddine, TEM diffraction study of Al2CuMg (S ’/S) precipitation in an Al-Li-Cu-Mg(Zr) alloy, Philos. Mag. 92 (2012) 1876–1889. doi:10.1080/14786435.2012.659288.
[40] B. Gault, F. De Geuser, L. Bourgeois, B.M. Gable, S.P. Ringer, B.C. Muddle, Atom probe tomography and transmission electron microscopy characterisation of precipitation in an Al–Cu–Li–Mg–Ag alloy, Ultramicroscopy. 111 (2011) 683–689.
[41] V. Araullo-Peters, B. Gault, F. de Geuser, A. Deschamps, J.M. Cairney, Microstructural evolution during ageing of Al–Cu–Li–x alloys, Acta Mater. 66 (2014) 199–208. doi:10.1016/j.actamat.2013.12.001.
[42] A. Deschamps, B. Decreus, F. De Geuser, T. Dorin, M. Weyland, The influence of precipitation on plastic deformation of Al-Cu-Li alloys, Acta Mater. 61 (2013) 4010–4021.
[43] D. Ortiz, J. Brown, M. Abdelshehid, P. DeLeon, R. Dalton, L. Mendez, J. Soltero, M. Pereira, M. Hahn, E. Lee, J. Ogren, R. Clark, J. Foyos, O.S. Es-Said, The effects of prolonged thermal exposure on the mechanical properties and fracture toughness of C458 aluminum-lithium alloy, Eng. Fail. Anal. 13 (2006) 170–180. doi:10.1016/j.engfailanal.2004.10.008.
[44] B. Noble, S.J. Harris, S. Katsikis, K. Dinsdale, Low temperature thermal stability of quaternary Al-Li-Cu-Mg-alloys, in: W.J. Poole, M.A. Wells, D.J. Lloyd (Eds.), Alum. Alloys 2006 Pts 1 2 Res. Innov. Technol., Trans Tech Publications Ltd, Zurich-Uetikon, 2006: pp. 209–214.
[45] S. Katsikis, B. Noble, S.J. Harris, Microstructural stability during low temperature exposure

of alloys within the Al-Li-Cu-Mg system, Mater. Sci. Eng. -Struct. Mater. Prop. Microstruct. Process. 485 (2008) 613–620. doi:10.1016/j.msea.2007.10.020.
[46] F. De Geuser, F. Bley, A. Deschamps, A new method for evaluating the size of plate-like precipitates by small-angle scattering, J. Appl. Crystallogr. 45 (2012) 1208–1218. doi:10.1107/S0021889812039891.
[47] A. Deschamps, F. De Geuser, Quantitative Characterization of Precipitate Microstructures in Metallic Alloys Using Small-Angle Scattering, Metall. Mater. Trans. -Phys. Metall. Mater. Sci. 44A (2013) 77–86. doi:10.1007/s11661-012-1435-7.
[48] D. Tsivoulas, J.D. Robson, C. Sigli, P.B. Prangnell, Interactions between zirconium and manganese dispersoid-forming elements on their combined addition in Al–Cu–Li alloys, Acta Mater. 60 (2012) 5245–5259. doi:10.1016/j.actamat.2012.06.012.
[49] K.S. Ghosh, K. Das, U.K. Chatterjee, Kinetics of solid-state reactions in Al-Li-Cu-Mg-Zr alloys from calorimetric studies, Metall. Mater. Trans. -Phys. Metall. Mater. Sci. 38A (2007) 1965–1975. doi:10.1007/s11661-007-9250-2.
[50] K.S. Ghosh, K. Das, U.K. Chatterjee, Calorimetric studies of 8090 and 1441 Al–Li–Cu–Mg–Zr alloys of conventional and retrogressed and reaged tempers, J. Mater. Sci. 42 (2007) 4276–4290. doi:10.1007/s10853-006-0619-1.
[51] T. Dorin, A. Deschamps, F. De Geuser, W. Lefebvre, C. Sigli, Quantitative description of the T1 formation kinetics in an Al–Cu–Li alloy using differential scanning calorimetry, small-angle X-ray scattering and transmission electron microscopy, Philos. Mag. 94 (2014) 1012–1030. doi:10.1080/14786435.2013.878047.
[52] M.J. Starink, N. Gao, N. Kamp, S.C. Wang, P.D. Pitcher, I. Sinclair, Relations between microstructure, precipitation, age-formability and damage tolerance of Al-Cu-Mg-Li (Mn, Zr, Sc) alloys for age forming, Mater. Sci. Eng. -Struct. Mater. Prop. Microstruct. Process. 418 (2006) 241–249. doi:10.1016/j.msea.2005.11.023.
[53] C. Genevois, A. Deschamps, A. Denquin, B. Doisneau-cottignies, Quantitative investigation of precipitation and mechanical behaviour for AA2024 friction stir welds, ACTA Mater. 53 (2005) 2447–2458. doi:10.1016/j.actamat.2005.02.007.
[54] M. Starink, S. Wang, The thermodynamics of and strengthening due to co-clusters: General theory and application to the case of Al-Cu-Mg alloys, Acta Mater. 57 (2009) 2376–2389. doi:10.1016/j.actamat.2009.01.021.
[55] H. Okuda, I. Tanaka, T. Matoba, K. Osamura, Y. Amemiya, In-situ and simultaneous synchrotron-radiation small-angle and 100 scattering experiments on the low-temperature structure in As-quenched Al-Li alloy during heating, Scr. Mater. 37 (1997) 1739–1744.
[56] H. Okuda, I. Tanaka, T. Matoba, K. Osamura, Y. Amemiya, Nature of an endothermic peak of As-quenched Al-11.8 mol%Li alloys, Mater. Trans. JIM. 39 (1998) 62–68.
[57] A. Deschamps, C. Sigli, T. Mourey, F. de Geuser, W. Lefebvre, B. Davo, Experimental and modelling assessment of precipitation kinetics in an Al–Li–Mg alloy, Acta Mater. 60 (2012) 1917–1928. doi:10.1016/j.actamat.2012.01.010.
[58] F. De Geuser, B. Malard, A. Deschamps, Microstructure mapping of a friction stir welded AA2050 Al–Li–Cu in the T8 state, Philos. Mag. 94 (2014) 1451–1462. doi:10.1080/14786435.2014.887862.
[59] A. Deschamps, F. De Geuser, On the validity of simple precipitate size measurements by Small-Angle Scattering in metallic systems, J. Appl. Crystallogr. (2011).
[60] C. Genevois, A. Deschamps, P. Vacher, Comparative study on local and global mechanical properties of 2024 T351, 2024 T6 and 5251 0 friction stir welds, Mater. Sci. Eng. Struct. Mater. Prop. Microstruct. Process. A415 (2006) 162–170.
[61] J. Garland, J. Sanchez, CLUSTER VARIATION METHOD CALCULATION OF THE METASTABLE ALUMINUM LITHIUM PHASE-DIAGRAM, in: H. Chen, V. Vasudevan (Eds.), MINERALS, METALS & MATERIALS SOC, 1992: pp. 207–216.
[62] B. Noble, S.E. Bray, On the [alpha](Al)/[delta]'(Al3Li) metastable solvus in aluminium-lithium alloys, Acta Mater. 46 (1998) 6163–6171. doi:10.1016/S1359-6454(98)00263-8.

[63] A. Deschamps, T.J. Bastow, F. de Geuser, A.J. Hill, C.R. Hutchinson, In situ evaluation of the microstructure evolution during rapid hardening of an Al-2.5Cu-1.5Mg (wt.%) alloy, ACTA Mater. 59 (2011) 2918–2927. doi:10.1016/j.actamat.2011.01.027.
[64] C. Genevois, A. Deschamps, A. Denquin, B. Doisneau cottignies, Quantitative investigation of precipitation and mechanical behaviour for AA2024 friction stir welds, Acta Mater. 53 (2005) 2447–2458.
[65] E. Gumbmann, W. Lefebvre, F. De Geuser, C. Sigli, A. Deschamps, The effect of minor solute additions on the precipitation path of an AlCuLi alloy, Acta Mater. 115 (2016) 104–114. doi:10.1016/j.actamat.2016.05.050.

Figure(s)

Alloy	Cu	Li	Mg	Ag	Mn	Zr
Base	2.8	0.7	0.3	0.2	<0.01	0.14
High Mg	2.7	0.8	0.6	0.3	<0.01	0.14
High Li	2.3	1.4	0.3	0.3	0.3	<0.01

Table 1: Composition of investigated alloys (in weight%)

Ageing time	Precipitate radius (nm)	Integrated intensity ($Å^{-6}$)	Volume fraction (%)
1000h	3.7	0.0146	5.6
2000h	4.5	0.0205	7.8
3000h	4.9	0.028	10.3

Table 2: Characteristics of the precipitates formed during LTA in the high Li alloy obtained from the SAXS data

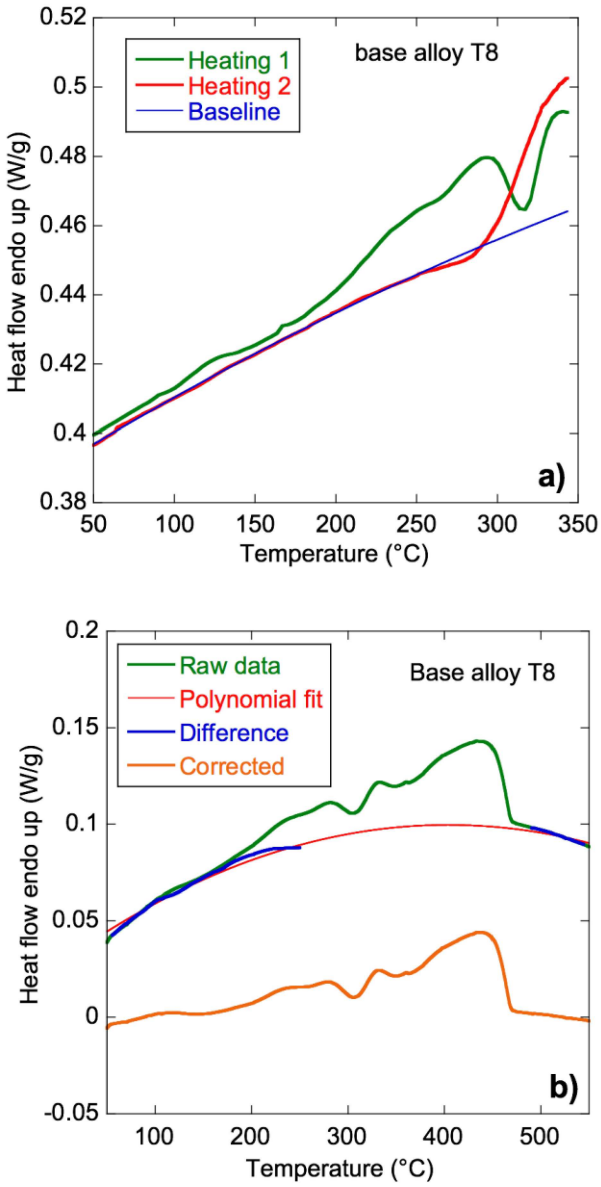

Figure 1: Differential scanning calorimetry baseline correction method (a) for the low temperature data and (b) for the full temperature scan

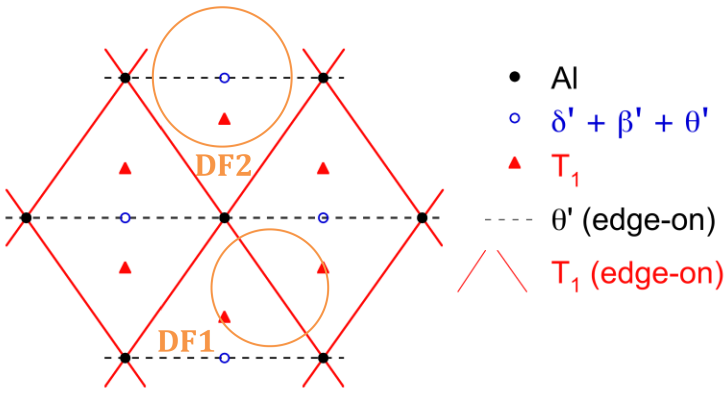

<110> matrix zone axis

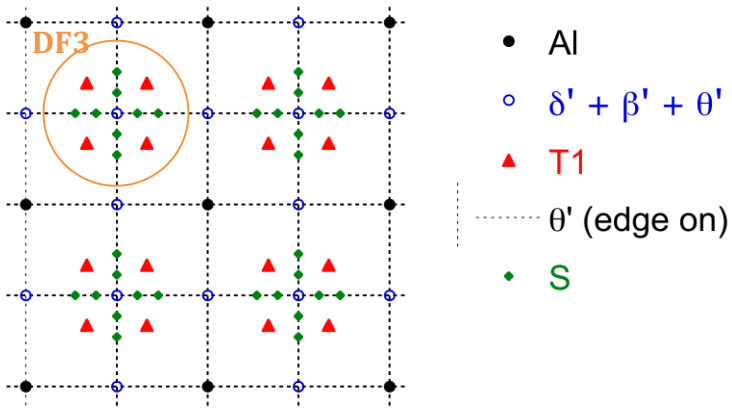

<100> matrix zone axis

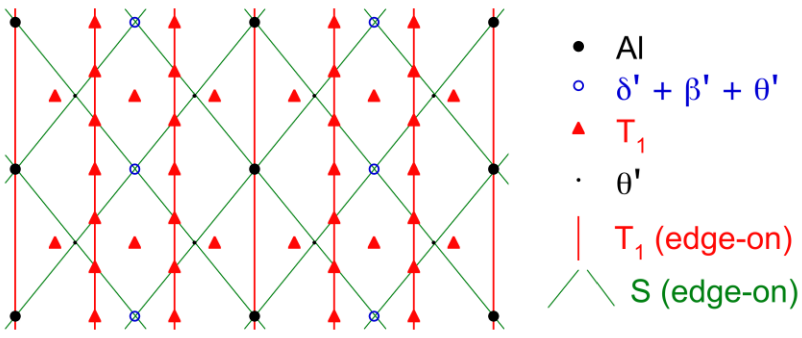

<112> matrix zone axis

Figure 2 : Scheme of the spots and streaks expected from the main precipitate phases in the three main zone axes.

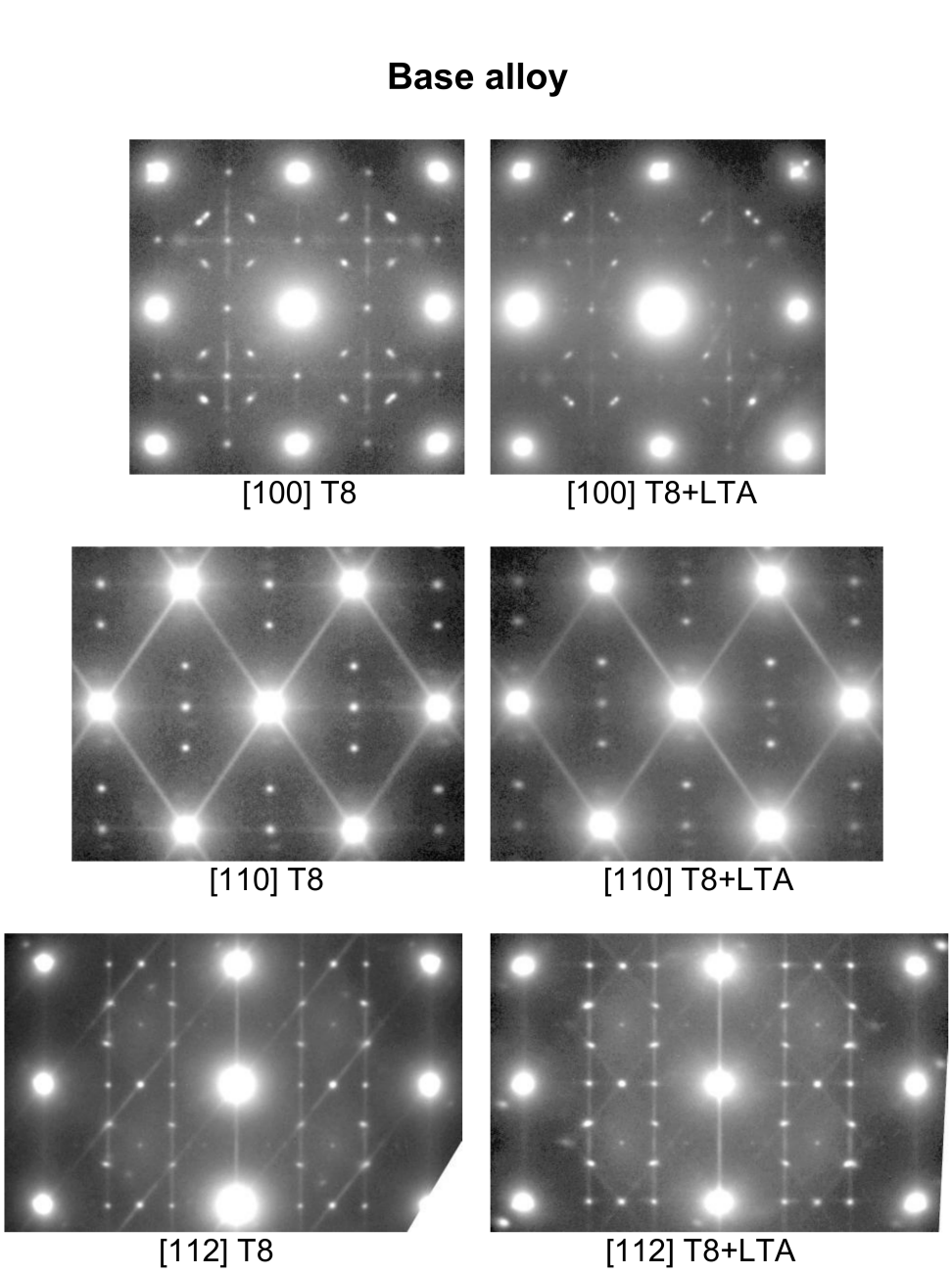

Figure 3 : Diffraction patterns in the T8 and T8+LTA conditions in the three zone axes for the base alloy.

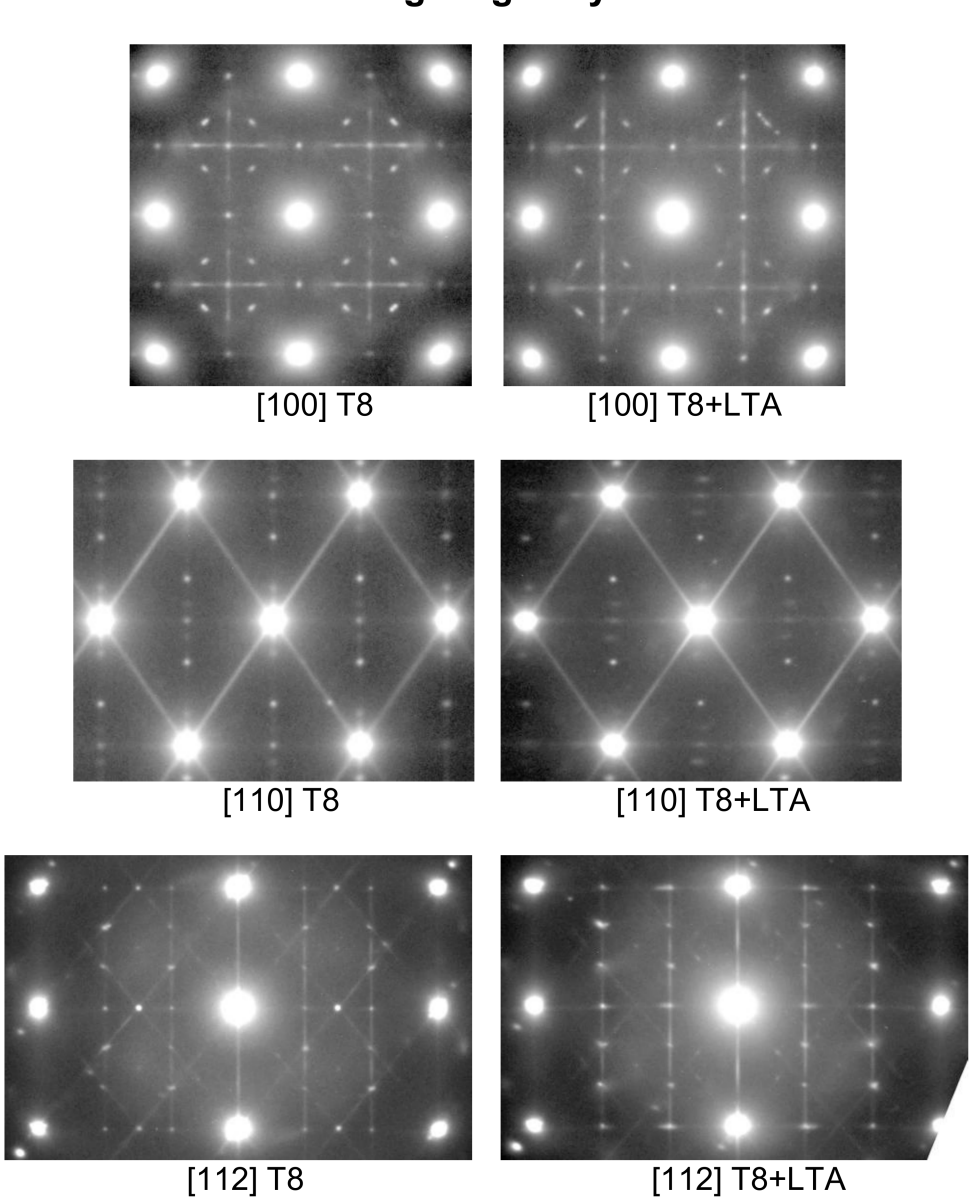

Figure 4 : Diffraction patterns in the T8 and T8+LTA conditions in the three zone axes for the high Mg alloy.

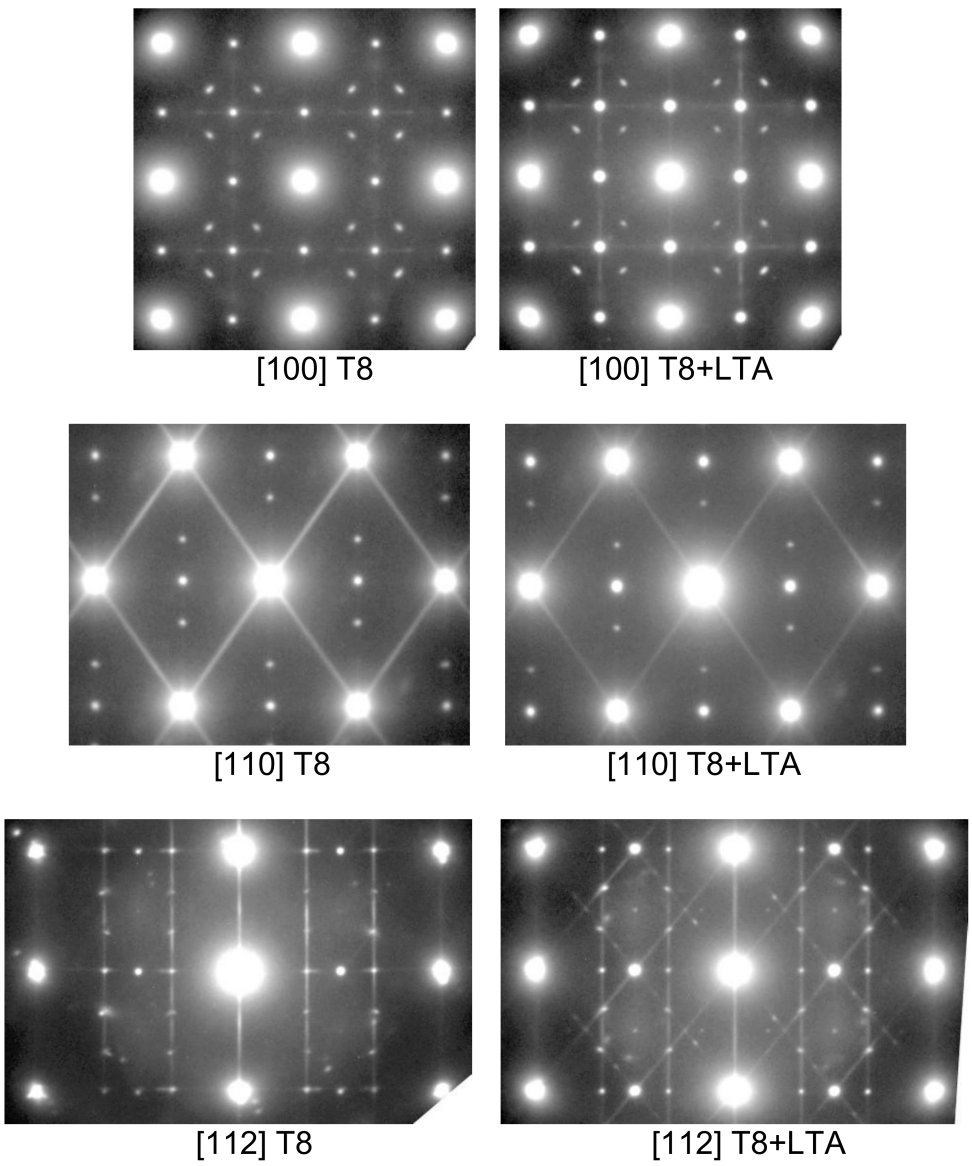

Figure 5 : Diffraction patterns in the T8 and T8+LTA conditions in the three zone axes for the high Li alloy.

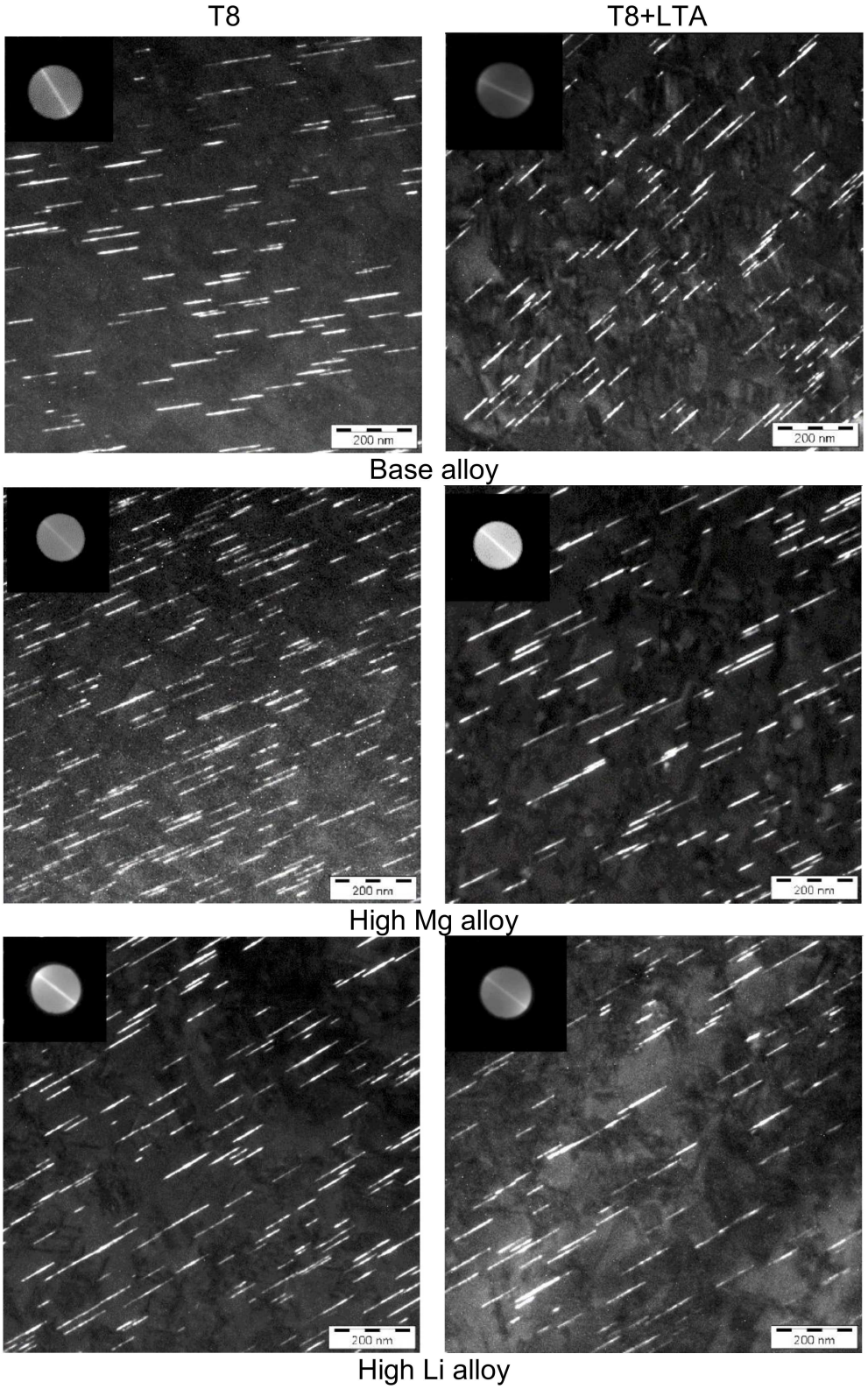

Figure 6 : Dark field transmission electron micrographs in <110> zone axis with the aperture in the DF1 position described in Figure 2.

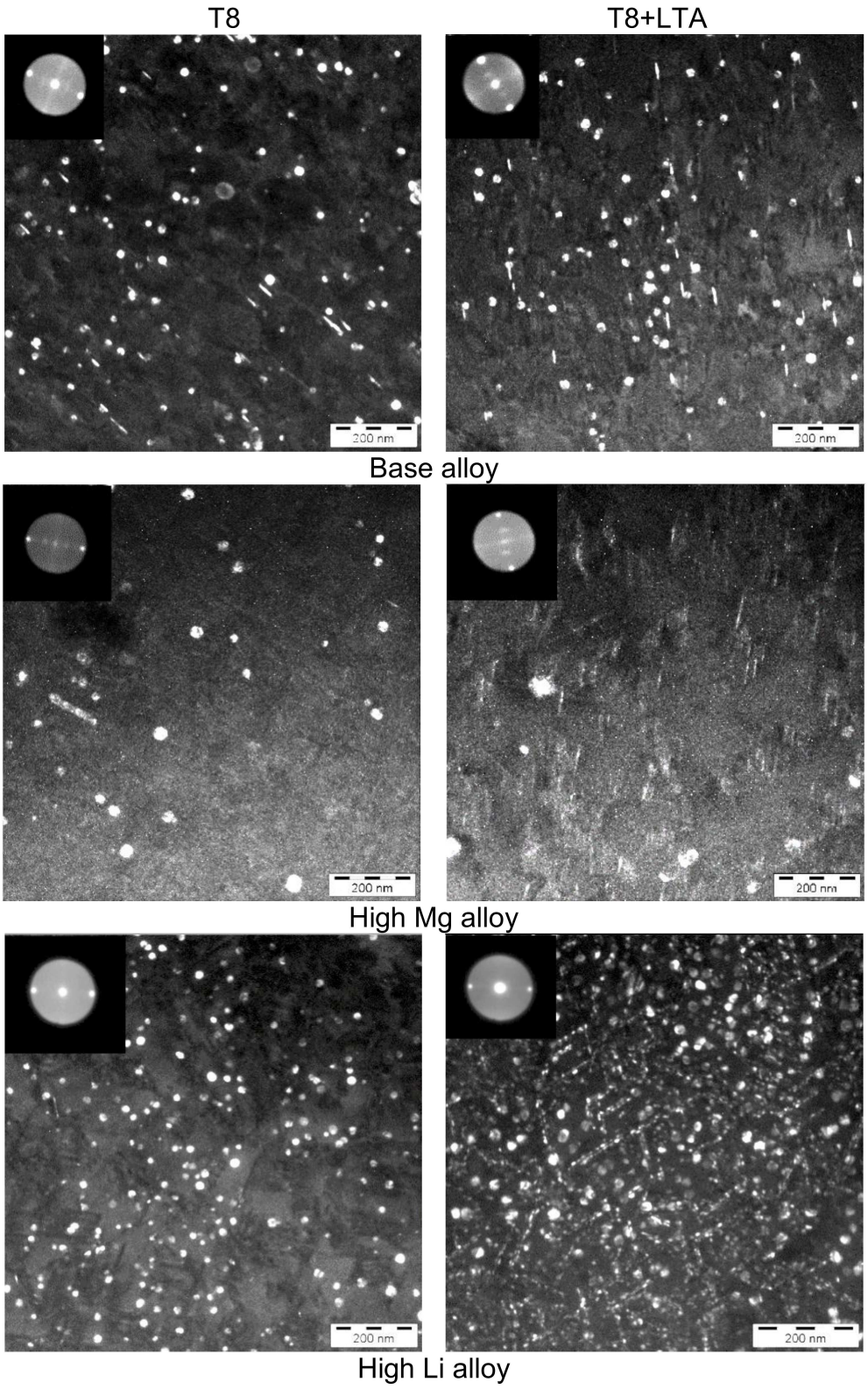

Figure 7 : Dark field transmission electron micrographs in <110> zone axis with the aperture in the DF2 position described in Figure 2.

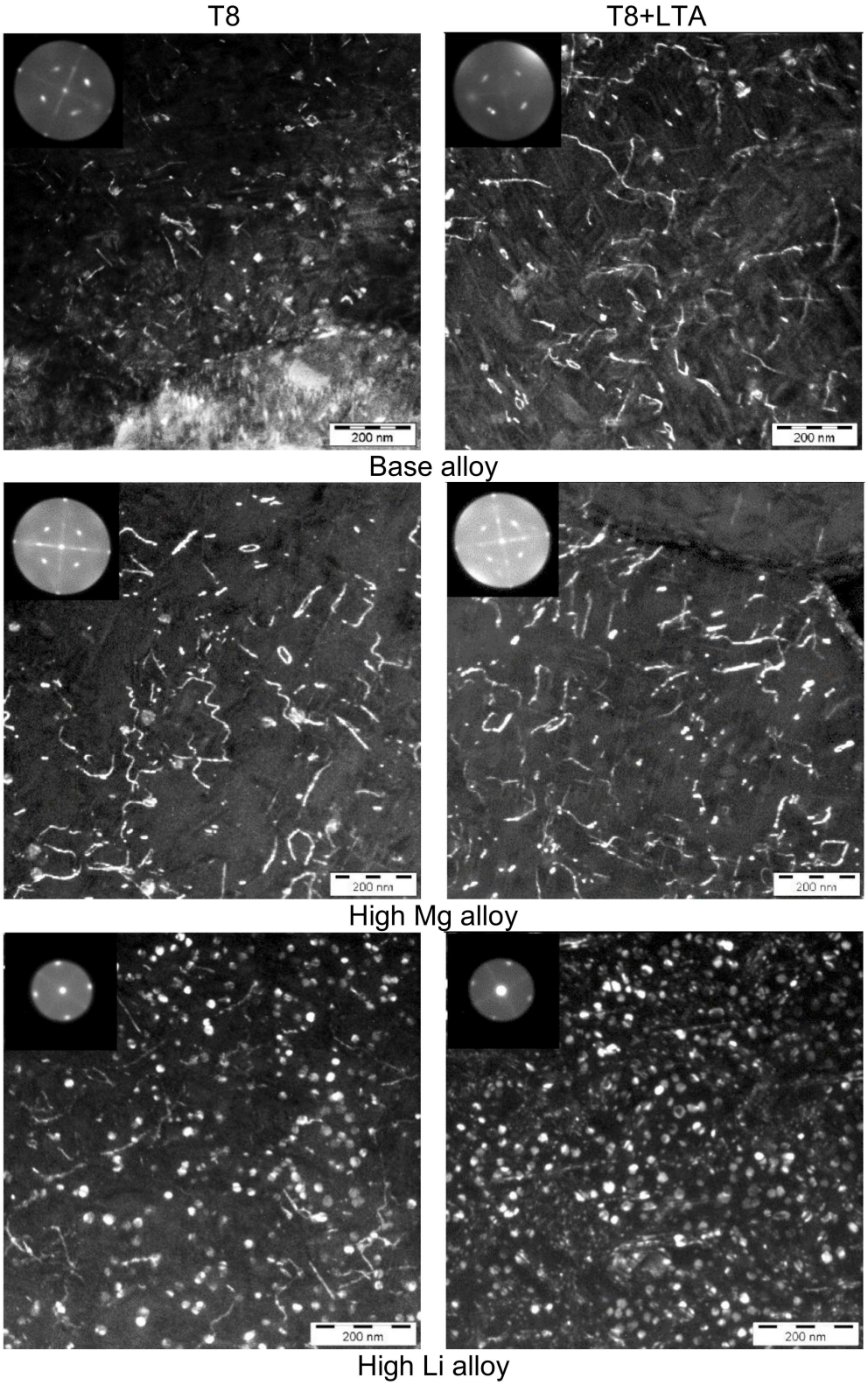

Figure 8: Dark field transmission electron micrographs in <100> zone axis with the aperture in the DF3 position described in Figure 2.

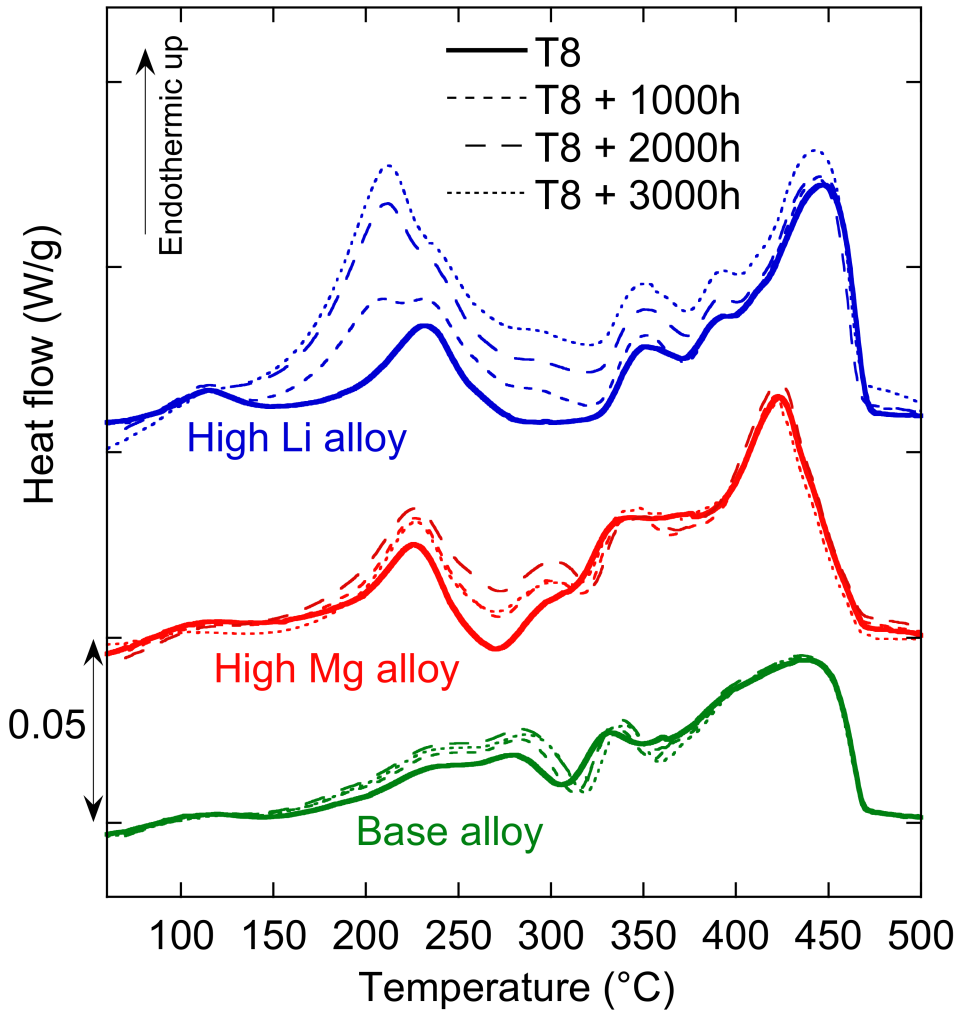

Figure 9 : DSC patterns for all alloy and ageing states (complete temperature scan)

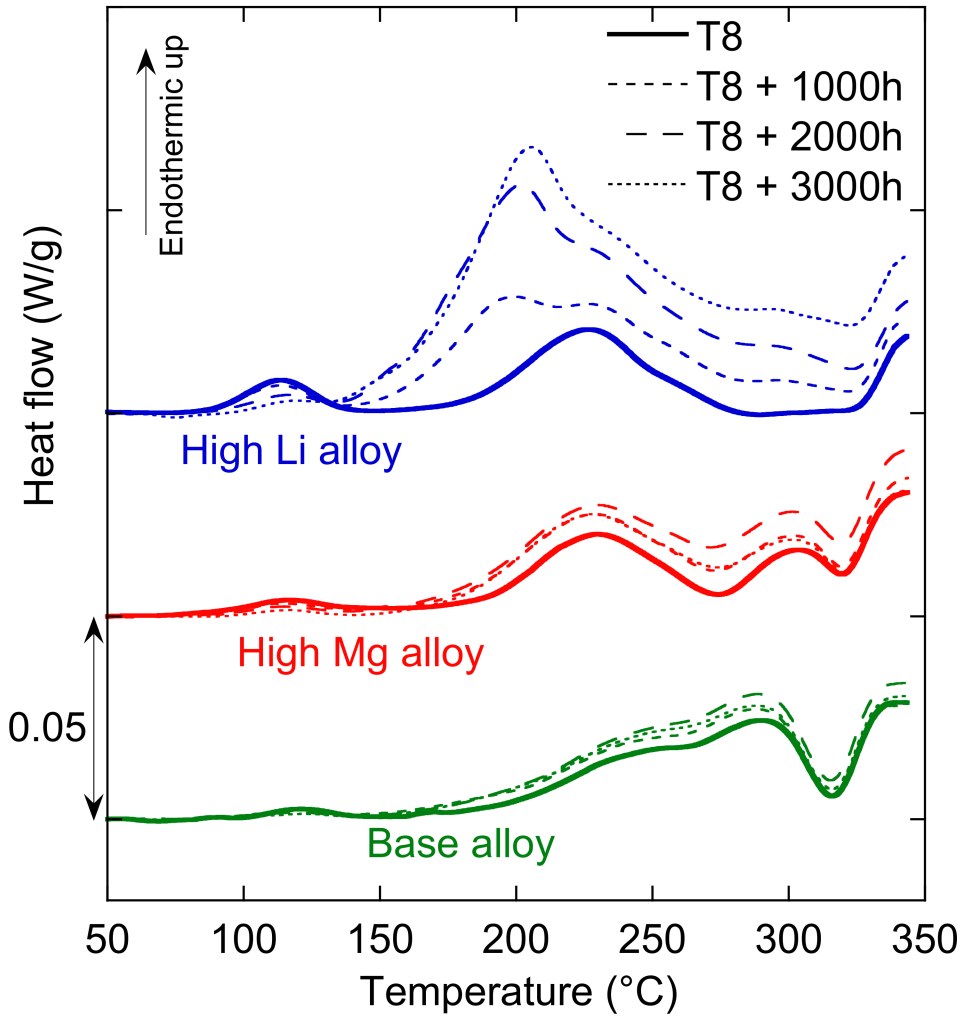

Figure 10 : DSC patterns for all alloys and ageing states (low temperature region)

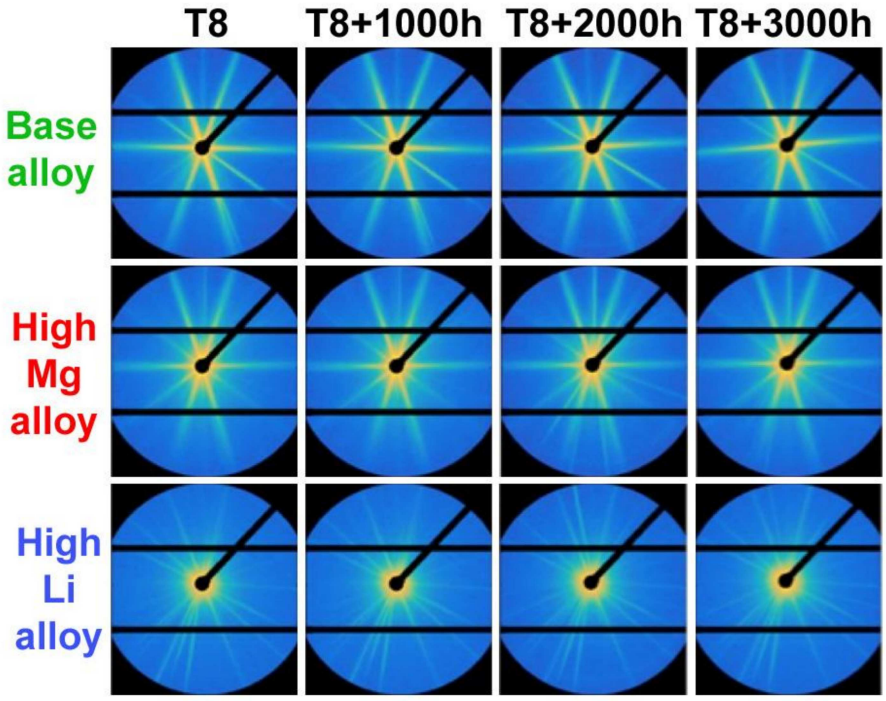

Figure 11 : SAXS images for all alloys and ageing states

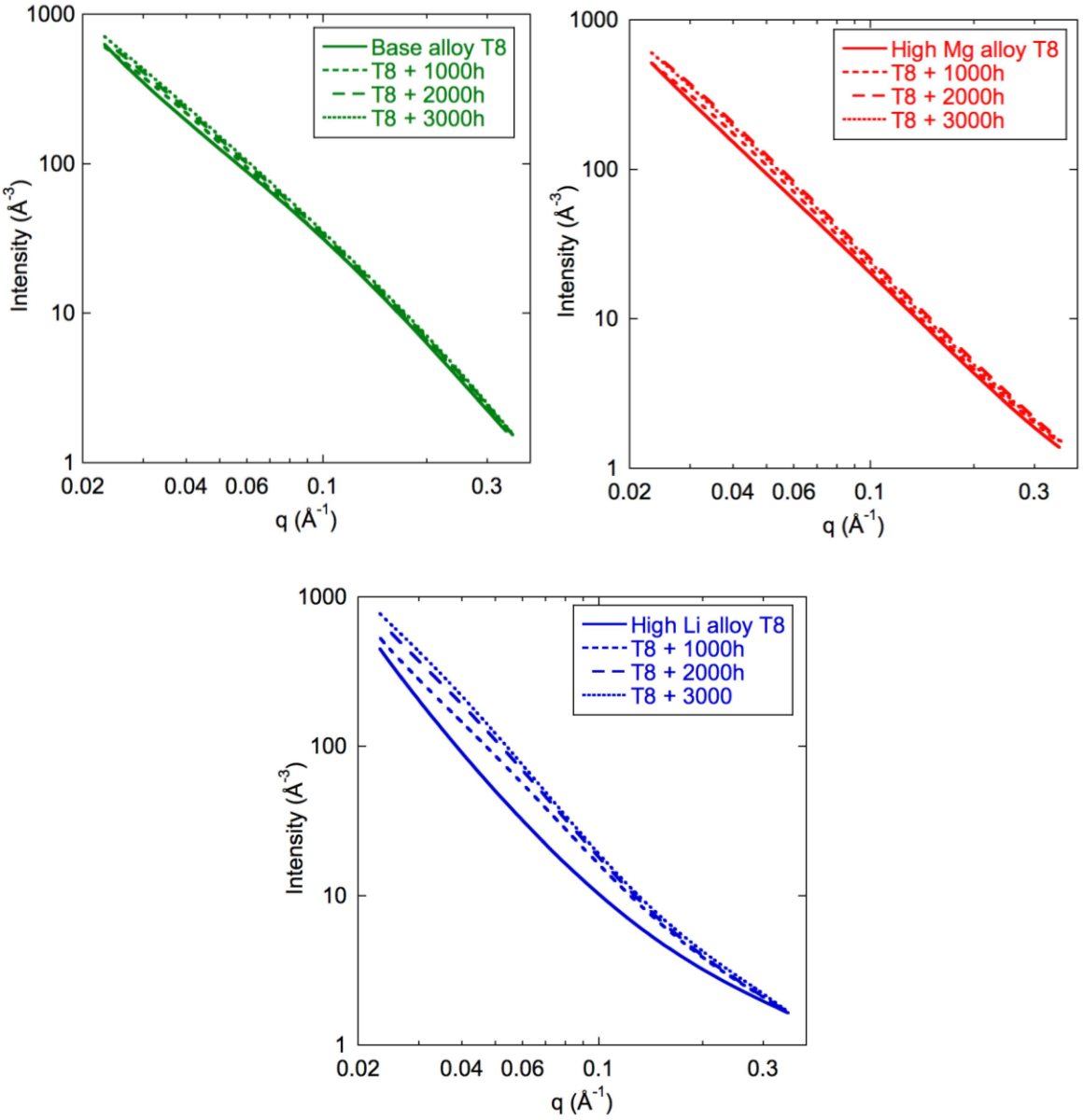

Figure 12: Radially averaged SAXS curves for all alloys and ageing states

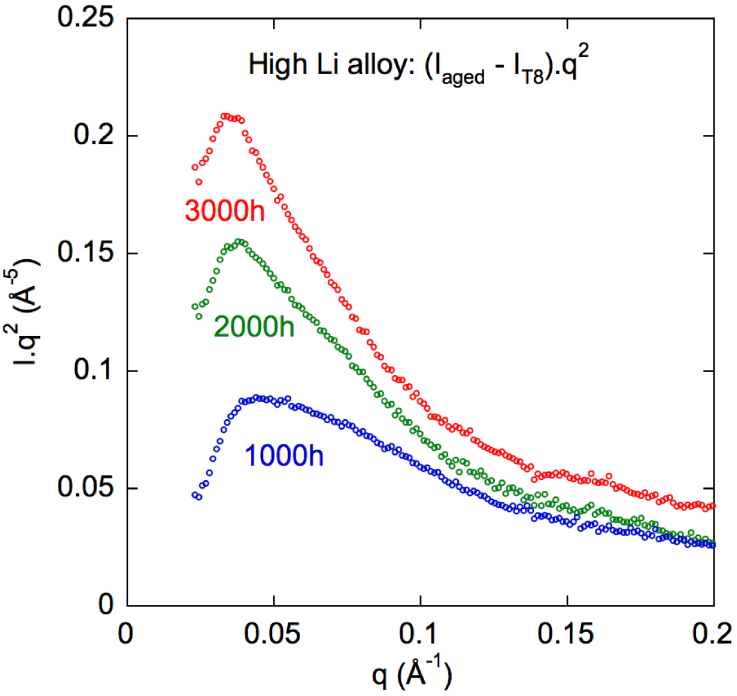

Figure 13: Kratky plot of the difference in SAXS intensity between the aged and initial T8 conditions for the high Li alloy

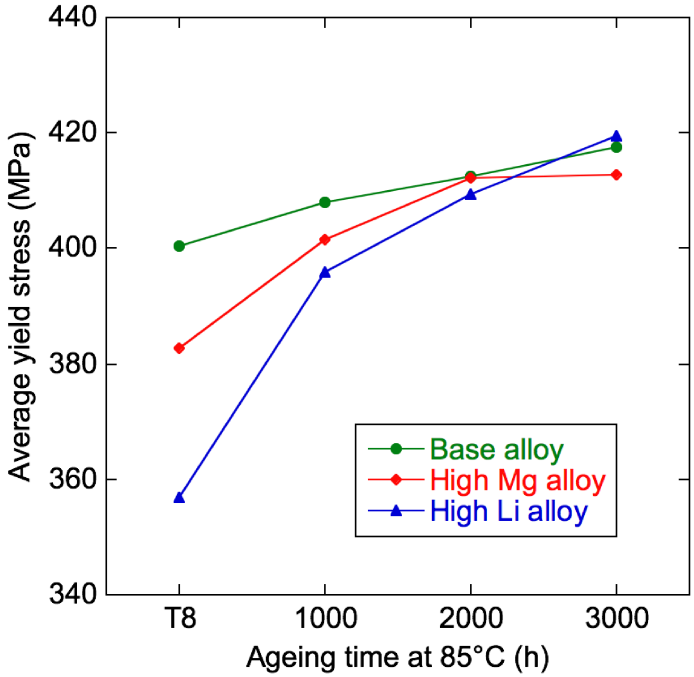

Figure 14: Evolution of the average of the yield stress between the L and LT loading directions for the three alloys as a function of the LTA time.